

# An interpretable wildfire spreading model for real-time predictions

K. Vogiatzoglou<sup>a</sup>, C. Papadimitriou<sup>a</sup>, K. Ampountolas<sup>a</sup>, M. Chatzimanolakis<sup>b</sup>,  
P. Koumoutsakos<sup>b</sup> and V. Bontozoglou<sup>a,\*</sup>

<sup>a</sup>Department of Mechanical Engineering, University of Thessaly, Volos, 38334, Greece

<sup>b</sup>Computational Science and Engineering Laboratory, School of Engineering and Applied Science, Harvard University, Cambridge, MA 02138, USA

## ARTICLE INFO

### Keywords:

Physical modeling  
Wildfire propagation  
Wind speed  
Fuel properties  
Fireline geometry

## ABSTRACT

Forest fires pose a natural threat with devastating social, environmental, and economic implications. The rapid and highly uncertain rate of spread of wildfires necessitates a trustworthy digital tool capable of providing real-time estimates of fire evolution and human interventions, while receiving continuous input from remote sensing. The current work aims at developing an interpretable, physics-based model that will serve as the core of such a tool. This model is constructed using easily understandable equations, incorporating a limited set of parameters that capture essential quantities and heat transport mechanisms. The simplicity of the model allows for effective utilization of data from sensory input, enabling optimal estimation of these parameters. In particular, simplified versions of combustion kinetics and mass/energy balances lead to a computationally inexpensive system of differential equations that provide the spatio-temporal evolution of temperature and flammables over a two-dimensional region. The model is validated by comparing its predictions and the effect of parameters such as flammable bulk density, moisture content, and wind speed, with benchmark results. Additionally, the model successfully captures the evolution of the firefront shape and its rate of spread in multiple directions.

## 1. Introduction

In recent years, the frequency and severity of natural disasters resulting from wildfires have witnessed an alarming rise. This trend is expected to persist in the future, primarily due to the combined effects of climate change and unfavorable human activities [25, 8]. Wildfires are destructive and rapidly spreading fires that engulf expansive areas covered in vegetation and constitute a major threat for communities at the wildland-urban interface (WUI) [34]. The primary concern revolves around the threat to human life, but the detrimental consequences of this natural hazard are evident across physical, social, and economic domains [19]. The most crucial information needed to protect lives and property and guide firefighter efforts is the rate of spread (ROS) of the firefront. Moreover, the fireline perimeter and area, along with firepower and intensity, represent essential quantities that are crucial to predict during situations of intense fire propagation [1].

Wildland fires are complex environmental phenomena, that involve multiple spatial and temporal scales and physical processes including the chemistry of fuel combustion, the physics of fluid flow and heat-mass transport [60, 57]. In particular, the fuel in forests and shrublands consists of particle-like materials (e.g., leaves, grass, twigs,

\*Corresponding author

✉ kvogiatzoglou@uth.gr (K. Vogiatzoglou); costasp@uth.gr (C. Papadimitriou); k.ampountolas@uth.gr (K. Ampountolas); mchatzimanolakis@seas.harvard.edu (M. Chatzimanolakis); petros@seas.harvard.edu (P. Koumoutsakos); bont@uth.gr (V. Bontozoglou)

ORCID(s):

and pine needles) of varying size, composition, and humidity. The heterogeneity of the biomass fuel in a forest area can be described as a random field, inserting a probabilistic character into the flame's direction. The heating of the fuel particles that initiates combustion is evidently provided by radiation and convection, though their relative contributions are under debate [24, 27]. Heat convection is influenced by airflow above the plant canopy dictated by local meteorological conditions and terrain morphology [30, 31], and in addition affected by convection currents triggered by flame instabilities [23].

Although numerous models have been proposed over the years to develop hypotheses on how fire grows and spreads, there are still many questions concerning the physics underlying these phenomena [54]. Models aiming at the prediction of wildland fire dynamics, and in particular the rate of spread, may be classified into three categories: At the simplest –and most operation-oriented– end are models that propose empirical functional relations between the ROS and parameters such as wind speed, fuel bulk density, and humidity [64, 63, 20, 40, 15, 47]. At the other end of the spectrum are three-dimensional computational fluid dynamics (CFD) simulations that aim at fully describing all physical phenomena over a large range of scales. Typical examples are the so-called multiphase models [57] that analyze at the lengthscale of tens of centimeters and provide detailed information on the combustion process [44], the wildfire models at the scale of meters such as FIRETEC [37, 6] and the atmospheric boundary layer models that discretize at the lengthscale of hundreds of meters and provide an overall view of the fire progression [38, 13]. The CFD models are computationally intensive, so their main contribution at present is in the elucidation of the governing physical mechanisms operative at the various spatial scales.

Between empirical functional relations and CFD tools, a number of simple but interpretable models have been proposed that describe the essential physics while being computationally tractable with the aim of providing real-time predictions [14, 39, 56, 4]. A key challenge for these models is the ability to include a multitude of parameters that affect the firefront progression, such as fuel density, composition, humidity, wind speed/direction and terrain morphology. More importantly, such models should be capable of reliable predictions subject to significant uncertainties, such as those imposed by canopy heterogeneity and the time-variation of weather conditions.

Here, we propose a model that entails simplified forms of mass and energy balances that are averaged over the plantation height. The model is built around a small number of interpretable parameters that correspond to dominant physical quantities or transport mechanisms. The model is designed to be utilized in real-time during an active fire, continuously gathering feedback through remote sensing techniques such as infrared cameras, weather radar, sensors, and satellites positioned in orbit or geostationary satellites [41, 35, 48]. In this context, a sequence of real-time predictions and comparisons with actual fire evolution will permit optimum parameter estimation, taking into account all the aforementioned uncertainties. We argue that the model provides a useful framework to support risk-informed decisions in the management of wildfires to help safeguard communities and natural resources.

In this paper we present model validation studies and compare model predictions with one and two-dimensional benchmark problems for the propagation of the firefront. The paper is structured as follows: The model derivation is described in Section 2. Section 2.1 introduces the simplified mass balances and reaction kinetics that approximate the real combustion processes, while Section 2.2 formulates the simplified energy balance in terms of the defined dispersion and convection coefficients, Section 2.3 introduces the effect of wind and Section 2.4 summarizes the model equations and clarifies the numerical implementation. In Section 3 the model is validated and used to predict results, first for one-dimensional fire propagation (straight frontline), and then for two-dimensional propagation from a localized or an extended ignition site. Finally, conclusions are drawn and future refinements are outlined in Section 4.

## 2. Modeling

### 2.1. Problem setup and mass balances

The proposed model incorporates the main physical mechanisms that are known to affect the rate of spread of a fire front, including reaction kinetics for water evaporation and wood combustion, heat transfer by convection and dispersion due to the motion of the gaseous phase (air/flue gases) through the plantation, and heat loss to the ambient by free convection and radiation.

We consider a field extending in the  $x$ - and  $y$ -direction, covered by a plantation of uniform height  $H$  ([=] m). Following standard convention [50], the bulk density of solid material,  $m_{s,0} = \alpha\rho_s$  ([=]  $\text{kg/m}^3$ ), is defined as the product of the volume fraction or packing ratio of solid,  $\alpha$  ([=]  $\text{solid m}^3/\text{total m}^3$ ), and the material density,  $\rho_s$  ([=]  $\text{kg/m}^3$ ). For example,  $\rho_s = 700 \text{ kg/m}^3$  for *Quercus coccifera* (an oak native to the Mediterranean region) and  $500 \text{ kg/m}^3$  for *Brachypodium ramosum* (a perennial grass native to Europe and Asia). The solid phase consists of two components: water and combustibles, the latter including non-aqueous volatiles (e.g., CO, CO<sub>2</sub>, NO<sub>x</sub>, VOC) and char. Thus,  $m_{s,0} = m_{s1,0} + m_{s2,0}$ , where  $m_{s1,0}/m_{s,0}$  is the original water content of the wood and  $m_{s2,0}/m_{s,0}$  the initial content of combustibles. Equivalently, the fuel moisture content (FMC), defined traditionally on a dry basis, is  $\text{FMC} = 100(m_{s1,0}/m_{s2,0})$ . Water content is typically classified as the humidity of live and/or dead plants. While the former varies mainly with plant type and time of the year, the latter is a function of air humidity and fuel size (the smaller the fuel particle, the faster it equilibrates with air humidity). With decreasing moisture content, the fuel is more flammable, and the fire spreads faster [51, 43].

During the combustion process, the remaining mass of solid material is  $m_s(x, y, t) = m_{s1}(x, y, t) + m_{s2}(x, y, t)$ . The rest of the field volume is the gaseous phase, whose mass,  $m_g$  ([=]  $\text{kg/m}^3$ ), increases with time due to the conversion of solid material into gaseous products. Thus, the conservation of total mass for a closed system, gives:

$$m_s + m_g = \alpha\rho_s + (1 - \alpha)\rho_g, \quad (1)$$

where  $\rho_g$  ( $[=] \text{ kg/m}^3$ ) is a representative gas density. Equation (1) may be written in dimensionless form by defining the remaining mass fraction of water,  $S_1 = m_{s,1}/m_{s,0}$  (endothermic fuel mass fraction), and combustibles,  $S_2 = m_{s,2}/m_{s,0}$  (exothermic fuel mass fraction), with  $S = S_1 + S_2$  (solid total fuel mass fraction), and also  $S_g = m_g/m_{s,0}$ . Thus:

$$S + S_g = 1 + \frac{1-\alpha}{\alpha} \lambda, \quad (2)$$

where  $\lambda$  is the density ratio  $\rho_g/\rho_s$ . We remark that parameter  $\alpha$  is a small number, typically of order  $10^{-3}$  [49].

In general, flame progression represents constant combustion that is influenced mostly by characteristics of the biomass fuel, such as moisture, surface roughness, and geometry. However, not only the combustible material but also the weather and the rest of the environmental conditions inside and around the canopy can either enhance or reduce fire intensity and progression rate. As a simplified description of a very complex set of chemical and physical processes [59], combustion may be considered to initiate with fuel dehydration, followed by pyrolysis and charring reactions, and conclude with oxidation reactions. While dehydration is endothermic, the start of pyrolysis reactions ( $T > 550\text{-}600 \text{ K}$ ) marks the onset of the flammable exothermic part [53, 17]. However, it is mainly in the last stage that the environmental conditions (turbulence, buoyant instabilities) play a key role. They may allow or prevent oxygen delivery to the burning fuel (resulting for example in glowing or smoldering fire oxidation [52]), and transfer heat to adjacent fuel, thus spreading the fire.

The wood dehydration and disintegration/combustion processes are modeled by two consecutive reactions, following first-order Arrhenius kinetics. Thus, the variation in water content with time is expressed as follows:

$$\frac{\partial S_1}{\partial t} = -S_1 r_1, \quad (3)$$

where

$$r_1 = c_{s1} e^{-\frac{b_1}{T}}, \quad (4)$$

with  $T$  ( $[=] \text{ K}$ ) representing the temperature of the fire layer, while parameters  $c_{s1}$  ( $[=] \text{ s}^{-1}$ ) and  $b_1$  ( $[=] \text{ K}$ ) may be used to quantify differences in behavior between dead and live moisture content [51]. A similar expression, with different constants, is used for the rate,  $r_2$ , of the burning process. However, in this case, the reaction rate is limited not only by the low temperature but also by a lack of oxygen [36]. Considering the two resistances in series, the final reaction rate is modeled as:

$$r_{2t} = \frac{r_2 r_m}{r_2 + r_m}, \quad (5)$$

where  $r_m$  ([=] s<sup>-1</sup>) is the rate of oxygen arrival to the burning solid. Finally, the temporal variation of combustibles is given by:

$$\frac{\partial S_2}{\partial t} = -S_2 r_{2t} = -S_2 \frac{c_{s2} e^{-\frac{b_2}{T}} r_m}{c_{s2} e^{-\frac{b_2}{T}} + r_m}. \quad (6)$$

The rate  $r_m$  is empirically determined to take values in the range [10<sup>-3</sup>, 10<sup>-2</sup>] (very small values result in fire extinction, very large values in unrealistically high flame temperatures). It is further expected to be an increasing function of wind speed and is presently approximated as,  $r_m = r_{m,0} + 0.004(\langle u \rangle - 1)$ , where  $r_{m,0} = 0.002$  s<sup>-1</sup> is an initial rate of oxygen arrival without wind, and  $\langle u \rangle$  ([=] m/s) is the local mean velocity across the plantation.

## 2.2. The energy balance

The energy balance is based on the assumption of local equilibrium [55], i.e., that the solid and gaseous phases have the same temperature. As a result, we may write the following equation for a volume of unit surface area and height  $H$ :

$$(m_s c_{ps} + m_g c_{pg}) \frac{\partial T}{\partial t} = -A_1 m_{s1} r_1 + A_2 m_{s2} r_{2t} - m_g c_{pg} \langle \mathbf{u} \rangle \cdot \nabla T + m_g c_{pg} \nabla \cdot (\mathbf{D}_{\text{eff}} \cdot \nabla T) - \frac{U}{H} (T - T_a). \quad (7)$$

Terms  $c_{ps}$  and  $c_{pg}$  ([=] J/kgK) are the heat capacities of the solid and gaseous phases, and  $A_1$ ,  $A_2$  ([=] J/kg) are the standard heats of the endothermic (water evaporation) and exothermic (pyrolysis and combustion) reactions. Term  $\langle \mathbf{u} \rangle$  is the mean velocity vector through the plantation, and the respective term is the convective contribution to the energy balance. Term  $\mathbf{D}_{\text{eff}}$  ([=] m<sup>2</sup>/s) is a dispersion coefficient, and  $U$  ([=] W/m<sup>2</sup>K) is an overall heat transfer coefficient for thermal losses to the environment, with  $T_a$  representing the ambient temperature and  $\nabla$  being the gradient operator.

The dispersion coefficient quantifies short-range heat transport by radiation, buoyant instabilities, and turbulent eddies. Radiation has long been considered the main transport mechanism [60, 56] for preheating to ignite the unburned fuel in front of the flame. However, this view was questioned [24], and it has been argued that instabilities caused by buoyant dynamics and unsteady convection (flame intermittency) dominate local transport [23] when the wind is high enough for the flame to be tilted. As  $\mathbf{D}_{\text{eff}}$  depends on the local velocity and a characteristic length in each direction [16], the dispersion coefficient is actually a (2x2) diagonal matrix with components  $D_{\text{eff},x}$  and  $D_{\text{eff},y}$ .

In order to model all the above contributions, the following form is adopted for the components of the dispersion coefficient:

$$D_{\text{eff},x} = D_{\text{rb}} + A_d \langle u_x \rangle L_x (1 - e^{-\gamma_d w_x}), \quad D_{\text{eff},y} = D_{\text{rb}} + A_d \langle u_y \rangle L_y (1 - e^{-\gamma_d w_y}), \quad (8)$$

where  $D_{rb}$  ([=] m<sup>2</sup>/s) is a representative constant that models buoyant dynamics and radiation,  $\langle u_x \rangle$ ,  $\langle u_y \rangle$  are the components of the mean velocity vector through the plantation, and  $A_d = 0.125$  is a selected dispersion constant. The first term in eq. (8) is the contribution of radiation and buoyancy and the second is the intensification of dispersion due to the wind. Two new length vectors,  $\mathbf{L}$  and  $\mathbf{w}$ , are introduced in eq. (8), which represent global lengthscales of the burning field and are updated every time-step. The vector  $\mathbf{L} = (L_x, L_y)$  is the distance from the location of global maximum temperature over the field,  $T_{max}$ , to the points in the  $x$ - and  $y$ -direction where temperature has dropped down to  $T = 0.1 T_{max} + T_a$ . Thus, it provides a measure of the width of the burning zone.

The term in parenthesis on the right hand side of eq. (8) expresses a mitigation of the effect of wind when the fire is spatially restricted, i.e., when the fireline is short [10]. It is known that the buoyant column of rising air partially obstructs the ambient air flow, and as a result pressure gradients develop that tend to redirect it. However, as has been shown by numerical simulations [6], a longer fireline will tend to allow more wind to push through, in contrast to a shorter fireline where the wind can be redirected more efficiently around the fire. In order to model this effect, the extent of the fireline in the  $x$ - and  $y$ -direction is expressed by the vector  $\mathbf{w} = (w_x, w_y)$ . This vector is determined at every time-step, by considering the temperature maxima in one direction (say  $x$ ) and their variation in the other direction (say  $y$ ). The resulting array,  $T_{max}(x_i, y_i)$ , is used to define the endpoints  $(x_A, y_A)$  and  $(x_B, y_B)$  of the fireline by the condition  $T_{max} > 550 \text{ K}$ . Then, the vector  $\mathbf{w}$  is defined as,  $w_x = |x_A - x_B|$ ,  $w_y = |y_A - y_B|$ . Varying the parameter  $\gamma_d$  ([=] m<sup>-1</sup>) in eq. (8) increases or decreases the fireline length at which the asymptotic limit (of the ROS of a long fireline) is practically reached.

Term  $U$  ([=] W/m<sup>2</sup>K) is an overall heat transfer coefficient that includes free convection and radiation, according to the expression:

$$U = h_{nc} + \varepsilon \sigma_b (T^2 + T_a^2) (T + T_a) = A_{nc} (T - T_a)^{1/3} + \varepsilon \sigma_b (T^2 + T_a^2) (T + T_a), \quad (9)$$

where  $A_{nc} \approx 0.2$  sums up terms from the correlation  $Nu_{nc} = 0.15 Gr^{1/3} Pr^{1/3}$ , valid for a horizontal hot surface and  $Gr > 10^7$ :

$$\frac{h_{nc} l_{nc}}{k} = 0.15 \left( \frac{g\beta}{\nu^2} \right)^{1/3} l_{nc} Pr^{1/3} (T - T_a)^{1/3} \Leftrightarrow h_{nc} = \left[ 0.15 \left( \frac{g\beta}{\nu^2} \right)^{1/3} Pr^{1/3} k \right] (T - T_a)^{1/3}. \quad (10)$$

Here,  $h_{nc}$  ([=] W/m<sup>2</sup>K) is the natural convection coefficient,  $\varepsilon$  is the emissivity,  $\sigma_b$  ([=] W/m<sup>2</sup>K<sup>4</sup>) is the Stefan Boltzmann constant,  $Nu_{nc}$  is the Nusselt number for natural convection,  $Gr$  is the Grashof number,  $Pr$  is the Prantl number,  $g$  ([=] m/s<sup>2</sup>) is the acceleration of gravity,  $\beta$  ([=] K<sup>-1</sup>) is the thermal expansion coefficient, which is equal to  $1/T$  for ideal gases,  $\nu$  ([=] m<sup>2</sup>/s) is the kinematic viscosity, and  $k$  ([=] W/mK) is the thermal conductivity of

**Table 1**

 Representative values of the parameters  $z_0$ ,  $\delta$  and  $\eta$  for a sparse and a dense canopy.

Parameter	Sparse Canopy	Dense Canopy
$z_0$	0.5 m	0.25 m
$\delta$	0.08 s	0.04 s
$\eta$	2	3

the hot gaseous products. The characteristic lengthscale for natural convection,  $l_{nc}$ , is usually taken as the ratio of cross-sectional area to perimeter of the hot surface, but it drops out in the high  $Gr$  limit.

### 2.3. Gas flow through the canopy

The transfer processes involved in the energy balance depend strongly on the motion of the gaseous phase through the canopy, which is expressed as a mean velocity,  $\langle u \rangle$ , across the plantation height,  $H$ . This velocity is determined by the wind speed above the plantation and the resistance to air motion exerted by the plantation. More specifically, [33, 30], the velocity field of the atmospheric boundary layer exerts a shear  $\tau$  ([=]  $\text{N/m}^2$ ) at the top of the canopy and imparts momentum to the underlying air. However, this momentum is dissipated not on the ground but throughout the canopy. In the following, the wind is defined by the velocity,  $u_{10}$ , at 10 m above the ground, as it is standard for meteorological measurements.

Following Inoue [33], (see fig. 1), the turbulent flow above the plantation is described by the following expression (law of the wall), and the nominal wind speed,  $u_{10}$ , is recovered by setting the height  $z = 10$  m:

$$u_v(z) = \frac{u_{v*}}{\kappa} \ln \left( \frac{z - d}{z_0} \right). \quad (11)$$

In eq. (11),  $\kappa = 0.41$  is the Karman's constant,  $z_0$  ([=] m) is the surface roughness at the top of the plantation [58] and  $u_{v*}$  ([=] m/s) is the friction velocity, which is evaluated by the substitution  $u_v(z = 10\text{m}) = u_{10}$ . The height  $d$  ([=] m) corresponds to the "nominal ground" as experienced empirically by the air flow above the plantation. In other words, the tentative extension of the logarithmic velocity profile inside the plantation goes to zero at  $z = d + z_0$ . This is also the location where the "nominal wall shear stress",  $\tau_w$ , applies. The height  $d$  decreases with wind speed, i.e., with increasing  $u_{10}$  the effect of the wind penetrates deeper inside the plantation. This tendency is currently approximated as follows:

$$d = (H - z_0) - \delta u_{10}, \quad (12)$$

where  $\delta$  ([=] s) and  $z_0$  are expected to vary with the thickness of the plantation (see table 1 for suggested representative values).

## An interpretable wildfire spreading model for real-time predictions

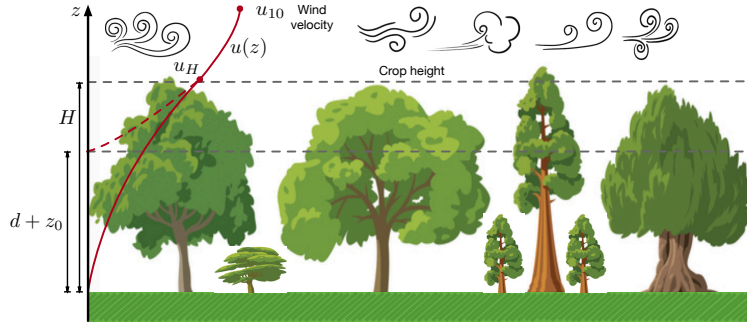


**Figure 1:** Wind profile inside and above the unburned plantation.

The actual velocity profile inside the plantation is determined by the following force balance over a differential section:

$$\frac{d\tau}{dz} = \rho_g C_d A_{pl} u^2, \quad (13)$$

where  $C_d \approx 0.25$  is an indicative value for the drag coefficient [28], and  $A_{pl}$  ( $[=] \text{m}^{-1}$ ) is the total surface area that exerts drag on the flow, per unit control volume ( $A_{pl}$  is usually expressed as the product  $A_{pl} = \alpha s_{pl}$ , where  $s_{pl}$  is the area per solid volume ratio [50]). Invoking the mixing-length hypothesis as a simple turbulence closure model, we may write:

$$\tau = l_m^2 \left( \frac{du}{dz} \right)^2, \quad (14)$$

where it has been argued [33, 30] that the fluid dynamics inside the plantation are satisfactorily captured by assuming a constant eddy size,  $l_m$  ( $[=] \text{m}$ ). Combining eq. (13) with eq. (14) and setting  $u(H) = u_H$  for the velocity at the top of the plantation leads to the following exponential profile inside the canopy:

$$u_v(z) = u_H e^{-\eta(1-z/H)}, \quad (15)$$

where

$$\eta = H \left( \frac{C_d A_{pl}}{2 l_m^2} \right)^{1/3}, \quad (16)$$



with typical values in the range  $\eta \in [2, 3]$ , see [33]. Finally, the mean velocity across the plantation height is calculated as:

$$\langle u_v \rangle = \frac{1}{H} \int_0^H u_v(z) dz = \frac{u_H}{\eta} (1 - e^{-\eta}). \quad (17)$$

The mean velocity  $\langle u_v \rangle$  calculated above describes the air motion ahead of the fire front and into the unburned region and is thus relevant to the rate of spread of the fire. However, behind the front, the air flow meets less drag resistance, as foliage and branches have been to a large extent eliminated by the fire. This latter air flow must thus be described by a higher mean velocity value,  $\langle u_b \rangle$ . Of course, the streamwise gradient of velocity thus imposed will generate pressure gradients that will drive the excess air flow around and over the fireline [6].

In order to express the aforementioned effect, we consider the logarithmic velocity profile over bare ground of roughness  $z_0$ :

$$u_b(z) = \frac{u_{b*}}{\kappa} \ln \left( \frac{z}{z_0} \right), \quad (18)$$

and define the mean velocity,  $\langle u_b \rangle$ , over the height  $H$  that corresponds to the unburned plantation ahead of the fire front. Thus:

$$\langle u_b \rangle = \frac{1}{H - z_0} \int_{z_0}^H u_b(z) dz = \frac{u_{b*}}{\kappa} \left[ \frac{H}{H - z_0} \ln \left( \frac{H}{z_0} \right) - 1 \right], \quad (19)$$

where the friction velocity,  $u_{b*}$ , is evaluated by the substitution  $u_b(z = 10m) = u_{10}$ . As  $\langle u_v \rangle$  is relevant to the intact, and  $\langle u_b \rangle$  to the totally burned-down canopy, we define the varying streamwise air velocity as a function of the remaining fraction of combustibles,  $x_c = S_2/S_{2,0}$ . In particular, we presently use a simple linear approximation, and thus the mean local velocity to be applied in eq. (7), is calculated as:

$$\langle u \rangle = \langle u_v \rangle + (\langle u_b \rangle - \langle u_v \rangle) (1 - x_c). \quad (20)$$

We note that the mean velocity  $\langle u \rangle$  is a vector quantity. However, in the case of horizontal topography (to which the present paper is restricted), the air velocity inside the burning area is always co-current with the wind. This is why no vector notation has been used in the above derivations.

## 2.4. Final form and numerical implementation of the model

Summarizing the above developments, the final form of the model, to be implemented numerically, is outlined below. It consists of eqs. (3) and (6) that describe the evaporation of water and the consumption of combustibles,

supplemented by the final dimensionless form of the energy balance, eq. (7), that –in the mathematical literature– is also known as an advection-diffusion-reaction equation:

$$\frac{\partial S_1}{\partial t} = -S_1 r_1 \quad (21)$$

$$\frac{\partial S_2}{\partial t} = -S_2 r_{2t} \quad (22)$$

$$\frac{\partial T}{\partial t} = \frac{c_1}{c_0} \left( D_{\text{eff},x} \frac{\partial^2 T}{\partial x^2} + D_{\text{eff},y} \frac{\partial^2 T}{\partial y^2} - \langle u_x \rangle \frac{\partial T}{\partial x} - \langle u_y \rangle \frac{\partial T}{\partial y} \right) - \frac{c_2}{c_0} S_1 r_1 + \frac{c_3}{c_0} S_2 r_{2t} - \frac{c_4}{c_0} U(T - T_a) \quad (23)$$

The coefficients  $c_i$  combine thermo-physical properties and are given below:

$$c_0(S, \alpha, \gamma, \lambda) = \alpha S + (1 - \alpha)\lambda\gamma + \alpha\gamma(1 - S) \quad (24)$$

$$c_1(S, \alpha, \gamma, \lambda) = (1 - \alpha)\lambda\gamma + \alpha\gamma(1 - S) = c_0 - \alpha S \quad (25)$$

$$c_2(\alpha, \lambda_1) = \alpha \lambda_1 \quad (26)$$

$$c_3(\alpha, \lambda_2) = \alpha \lambda_2 \quad (27)$$

$$c_4(\lambda_3) = 1/\lambda_3, \quad (28)$$

where  $\gamma = c_{pg}/c_{ps}$ ,  $\lambda_1 = A_1/c_{ps}$ ,  $\lambda_2 = A_2/c_{ps}$ ,  $\lambda_3 = H\rho_s c_{ps}$  and it is recalled that  $\lambda = \rho_g/\rho_s$ .

The set of eqs. (21), (22), and (23) is discretized by an explicit, finite difference scheme on a rectangular uniform grid with typical spacing  $\Delta x = \Delta y = 1$  m. First-order upwinding is used for the advection terms and second-order, central differences for the dispersion terms. The resulting system of temporal ODEs is solved by Adams–Bashforth methods [29] with time step  $\Delta t = 0.01$  s for stability [5]. The evolution of the dependent variables,  $T, S_1, S_2$ , is followed in time on the computational grid, and data are stored for every 1s. The computation is run on an AMD Ryzen Threadripper PRO 3995WX processor with 64 cores.

A localized temperature spike with  $T_{i,max} = 1200$  K is used as the initial condition, described either by a rectangular step-function of width 10 – 30 m, or by a Gaussian spike with typical standard deviation  $\sigma = 20$  m. As for the other two dependent variables, a uniform endothermic,  $S_{1,0}$ , and exothermic,  $S_{2,0}$ , fuel composition is considered across the domain. An open outflow boundary condition is implemented at the downstream boundaries, in order to allow the firefront to move smoothly out of the computational domain without significant backward influence [46, 18]. This condition essentially amounts to extending the validity of the discretized equations at the boundary nodes, using appropriate one-sided approximations for the spatial derivatives. The effectiveness of this condition is confirmed by the very good agreement with representative runs on a computational domain twice the regular size.

**Table 2**  
Representative values of the model parameters.

Parameter	Value	Parameter	Value	Parameter	Value	Parameter	Value
FMC	25%	$c_{ps}$ (J/kgK)	1800	$A_1$ (J/kg)	$22 \cdot 10^5$	$\sigma$ (m)	20
$H$ (m)	2	$c_{pg}$ (J/kgK)	1043	$A_2$ (J/kg)	$2 \cdot 10^7$	$C_d$	0.25
$T_a$ (K)	300	$c_{s1}$ (s <sup>-1</sup> )	30	$\sigma_b$ (W/m <sup>2</sup> K <sup>4</sup> )	$5.67 \cdot 10^{-8}$	$A_d$	0.125
$T_{i,max}$ (K)	1200	$c_{s2}$ (s <sup>-1</sup> )	40	$D_{rb}$ (m <sup>2</sup> /s)	0.1	$A_{nc}$	0.2
$\rho_s$ (kg/m <sup>3</sup> )	700	$b_1$ (K)	4500	$r_{m,0}$ (s <sup>-1</sup> )	0.002	$\alpha$	0.002
$\rho_g$ (kg/m <sup>3</sup> )	1	$b_2$ (K)	7000	$\gamma_d$ (m <sup>-1</sup> )	0.03	$\epsilon$	0.3

### 3. Model validation and results

#### 3.1. A representative one-dimensional simulation

Having developed a model for wildfire spreading, the next objective is to probe its behavior and compare its predictions to observations that are known from laboratory experiments and field studies.

The one-dimensional (1D) version of the model is first used to investigate the effects of some fuel properties (such as bulk density, moisture content, and particle size) and of wind speed and to demonstrate in a simple way the mechanisms that should be considered more carefully in a two-dimensional (2D) case. The 1D version corresponds to a very long fireline that moves uniformly in the longitudinal direction. As it is known that the rate of spread, ROS ([=] m/s) increases with the length  $w$  ([=] m) of the firefront [11, 37], the 1D model is expected to provide an upper limit to the actual ROS. The 2D version will be employed in the last subsection, in order to investigate the pattern of spread of the fire in various directions and the spatiotemporal evolution of the shape of the firefront.

The results for a representative case are shown in fig. 2, which correspond to the parameter values listed in table 2 and the values for a dense canopy in table 1. Figure 2(a) depicts the spatial variation of temperature for (a<sub>1</sub>)  $u_{10} = 3$  m/s and (a<sub>2</sub>)  $u_{10} = 10$  m/s at time instants  $t = 0, 800, 1600$  and  $2400$  s from the onset of the initial spikes (solid lines). The progression of the firefront with time is evident (dashed lines), and the ROS is readily calculated from the displacement of the temperature maximum and the corresponding time lag. Such a calculation indicates that sometimes the ROS increases gradually with time, a behavior reminiscent of fire's acceleration with size. Such a concept has been included in some prediction models, such as FARSITE or the Forestry Canada Fire Danger Group [50]. Aiming to overcome possible ambiguity, the ROS reported in the parametric investigations of this section is the mean value calculated from the crest progression between 1000 s and 1500 s from ignition.

Figure 2(b) depicts the spatial distribution of  $S_1$  and  $S_2$ , i.e., the dimensionless mass of water and combustibles remaining in the solid phase for (b<sub>1</sub>)  $u_{10} = 3$  m/s and (b<sub>2</sub>)  $u_{10} = 10$  m/s at the same time instants  $t = 0, 800, 1600$  and  $2400$  s from ignition. As expected, water has totally evaporated everywhere the flame has passed (blue lines) before the exothermic reaction takes place (red lines). However, varying amounts of combustible solid remain, depending

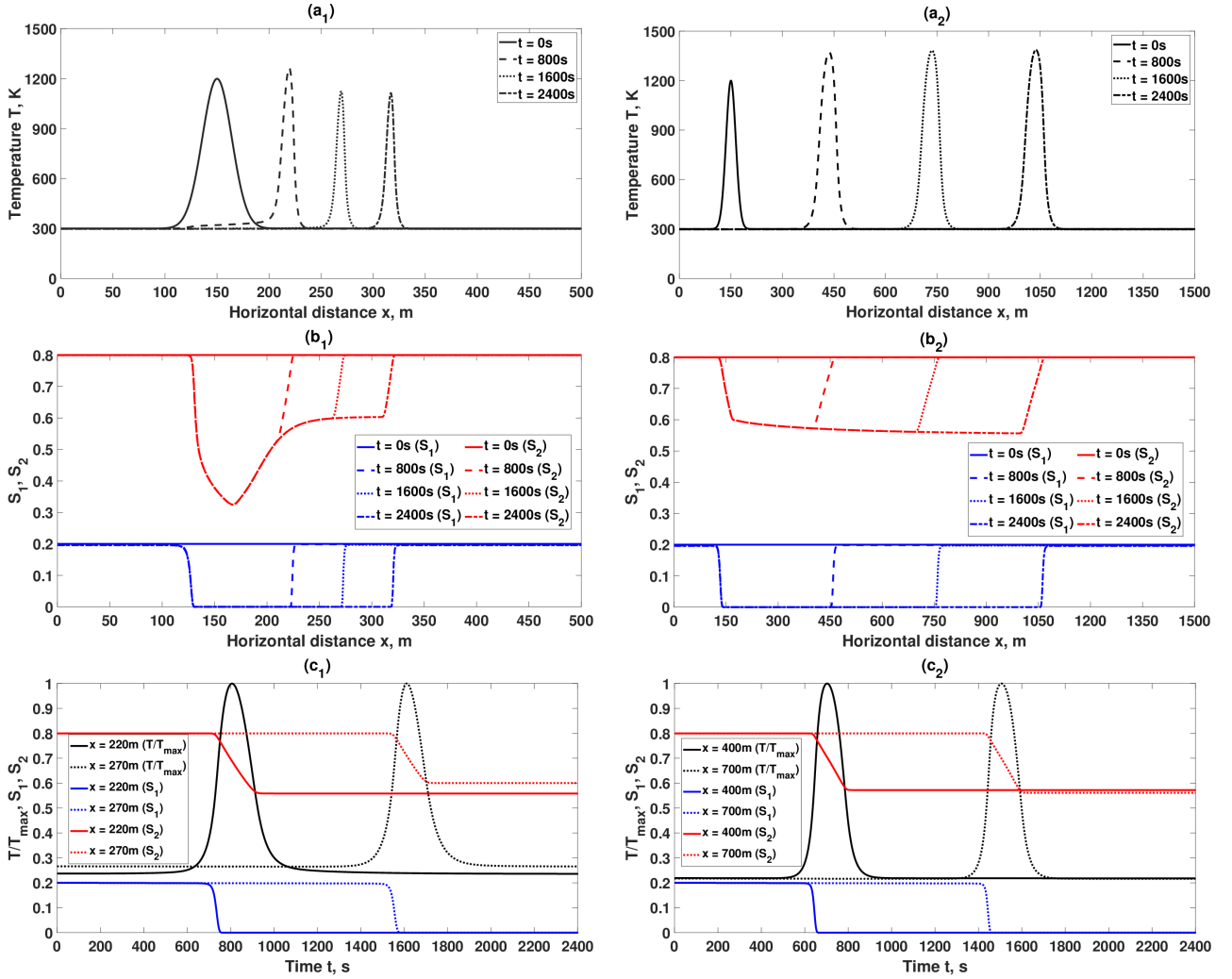


**Figure 2:** (a) The spatial distribution of temperature at time instants  $t = 0, 800, 1600$  and  $2400$  s, (b) the spatial distribution of  $S_1$  and  $S_2$  at the same time instants, (c) the temporal variation of dimensionless temperature  $T/T_{max}$ ,  $S_1$  and  $S_2$ . The subscript 1 (left column) is for  $u_{10} = 3$  m/s and the subscript 2 (right column) for  $u_{10} = 10$  m/s, while the localized ignition area is everywhere at  $x_0 = 150$  m from the origin.

on how fast the combustion proceeds and how efficiently the burned area is cooled down by the incoming wind. The increase in consumed combustibles with downstream distance explains the acceleration of the ROS that is sometimes observed: As fire moves ahead, it intensifies and burns more fuel during its passage, thus the firefront spreads faster. However, a steady-progressive state evidently establishes further downstream, which corresponds to an asymptotic limit  $S_2 \rightarrow S_{2,min}$ .

As an alternative representation of the same process, fig. 2(c) plots the three variables  $T/T_{max}$ ,  $S_1$  and  $S_2$  as functions of time, for (c<sub>1</sub>)  $u_{10} = 3$  m/s and (c<sub>2</sub>)  $u_{10} = 10$  m/s with  $t \in [0, 2400]$  s, at two different spatial locations,  $x = 220, 270$  m and  $x = 400, 700$  m respectively, from the ignition site (term  $T_{max}$  is the maximum temperature achieved at each location over time). The onset of combustion with the arrival of the firefront is evident, as well as the

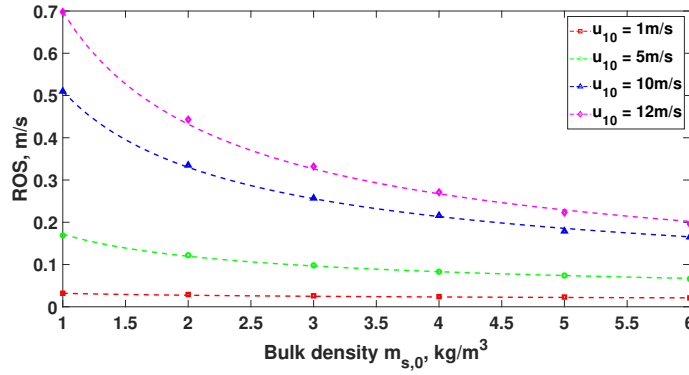


**Figure 3:** The ROS as a function of the fuel bulk density  $m_{s,0}$  for wind speeds,  $u_{10} = 1, 5, 10$  and  $12$  m/s. Points are simulation results and lines the best-fit inverse power law.

temperature decline behind the front, depicted by a tail that may be longer or shorter depending mainly on the wind speed. The remaining amount of combustibles,  $S_2$ , stabilizes to a constant value after some time, indicating extinction below the minimum ignition temperature. Again, it is evident that the remaining combustibles may decrease somewhat with downstream distance.

### 3.2. Fuel modeling flexibility: bulk density, moisture content and particle size

The model offers a number of parameters that may be combined to provide a realistic representation of the fuel's properties. The effect of some of these on the predicted ROS is considered next, and the predictions are set in perspective with experimental data and/or detailed, three-dimensional simulations in the literature.

The bulk density of solid material, defined as  $m_{s,0} = \alpha \rho_s$ , in terms of the volume fraction of solid,  $\alpha$ , and the material density,  $\rho_s$ , is known to have a systematic effect on the fire spread rate. More specifically, it has been observed [62, 7, 65, 9] that increasing bulk density leads to slower ROS. This behavior has been mathematically expressed by an inverse power law,  $ROS \sim m_{s,0}^{-\zeta}$ , which appears to satisfactorily describe both laboratory experiments and field observations [63, 20, 40, 62, 65, 9]. However, the proposed exponent varies widely among the above studies, moving in the range [0.23, 0.73].

The present model confirms the central role of bulk density. In particular, keeping all other parameters constant as outlined in tables 1, 2 the ROS is found to vary only with  $m_{s,0}$ , and not with  $\alpha$  or  $\rho_s$  independently. The inverse power law is also followed by the model, with the exponent,  $\zeta$ , actually being an increasing function of the air velocity,  $u_{10}$ , above the canopy. Indicative examples for  $u_{10} = 1, 5, 10$  and  $12$  m/s, and  $m_{s,0}$  in the range [1, 6] kg/m<sup>3</sup>, are shown in fig. 3. The exponent  $\zeta$  appears in the present model to follow the empirical fit,  $\zeta = 0.04(1 + u_{10})$ , with very good accuracy.

The increase in fuel moisture content is also known to result in slower ROS [40, 51] and to eventually lead to the extinction of the flame under sufficiently wet conditions. An exponential functionality of the form,  $ROS \sim e^{-\mu(FMC)}$ , has been repeatedly proposed [11, 21, 40, 43], but the exponent  $\mu$  is found to vary widely. In particular, it is higher when the correlation is based on dead moisture content and lower when using the mean value of dead and live moisture. Predictions of the present model, which is based on the total moisture content, are satisfactorily correlated by the same functional form and values of the exponent  $\mu$  in the range [0.013, 0.017], or even smaller for very low air velocities. The FMC that results in fire extinction is predicted to increase with bulk density and decrease with air velocity, i.e., a fire on wet fuel is more persistent at high bulk density and low air speed.

The effect of fuel particle size is also critical, as leaves and small-diameter sticks have larger surface-to-volume ratios and thus, burn faster than thick branches. This behavior may be quantified by the appropriate choice of the constants in the combustion kinetics. With reference to eq. (6), a characteristic burning time may be defined as:

$$t_c = -\frac{\ln(S_{2,f}/S_{2,0})}{c_{s2} e^{-b_2/T_c}}, \quad (29)$$

in terms of the initial,  $S_{2,0}$ , and the remaining,  $S_{2,f}$ , combustible material after time  $t_c$ . Taking this ratio as equal to 0.1 and using a characteristic burning temperature  $T_c \approx 1250$  K [61], gives the estimate  $t_c \approx 1000/c_{s2}$ . Values of  $c_{s2}$  in the range [5, 200]  $s^{-1}$  result in  $t_c$  in the range [200, 5] s. This range is very favorably compared with the fuel residence times for a variety of fuels in the extensive database presented in [45].

### 3.3. The role of wind

As evidenced already, the overlying wind speed is a key ingredient in determining the fire propagation speed and direction [64, 50, 55, 61, 3]. In the absence of wind, the fire is expected to spread symmetrically in all directions, with heat for ignition being transported by buoyant dynamics and radiation, as modeled by the term,  $D_{rb}$ , of the effective diffusivity. With increasing wind speed, fire propagation is accelerated in the direction of the wind and decelerated against it. Beyond a value of wind speed, propagation against the wind is arrested, and the backward front extinguishes [32].

In the present model, the effect of wind is introduced by a local mean velocity of the gaseous phase inside the plantation, as described in Section 2.3. Representative examples of front propagation are shown in fig. 4. Specifically, fig. 4(a) corresponds to zero wind speed,  $u_{10} = 0$  m/s, and exhibits symmetric propagation in both directions, as evidenced by the temperature profiles for time instants,  $t = 0, 1000$  and  $2000$  s. Introducing a small wind speed,  $u_{10} = 1$  m/s, in fig. 4(b) results in the acceleration of the wavefront moving with the wind and the deceleration of the front moving against the wind, as evidenced by the temperature profiles, now for time instants, at  $t = 0, 600$  and  $1200$  s. Increasing the wind speed further enhances the difference between the spread rates of the two fronts. Eventually,

## An interpretable wildfire spreading model for real-time predictions

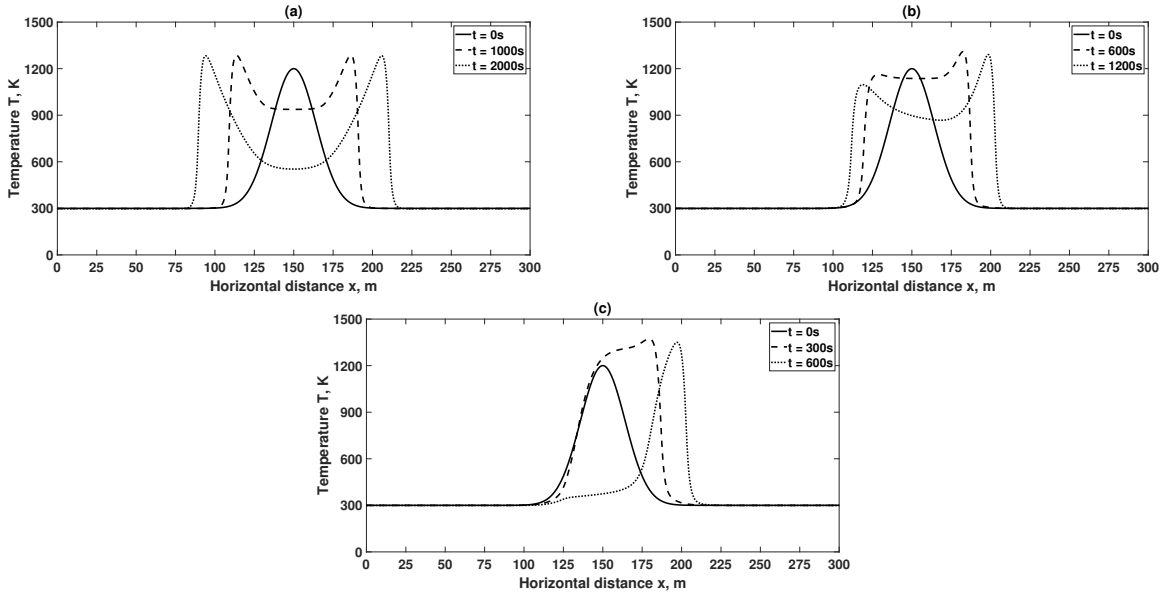


**Figure 4:** The spatial distribution of temperature at different time instants separated by  $\Delta t_s$  seconds. (a)  $u_{10} = 0$  m/s,  $\Delta t_s = 1000$  s, (b)  $u_{10} = 1$  m/s,  $\Delta t_s = 600$  s and (c)  $u_{10} = 2.5$  m/s,  $\Delta t_s = 300$  s.

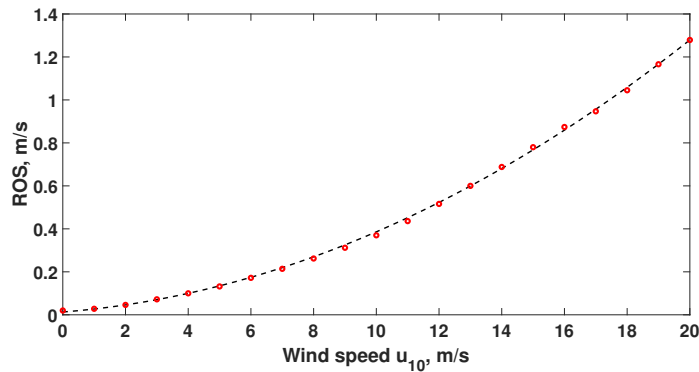


**Figure 5:** The ROS as function of the wind speed  $u_{10}$ , with all other parameters as listed in table 2. Points are simulation results and line the best-fit parabolic curve.

beyond  $u_{10} = 2.3$  m/s, the wind-opposed front blows off and the fire spreads only in the direction of the wind (see fig. 4(c) for  $u_{10} = 2.5$  m/s and  $t = 0, 300$ , and  $600$  s).

The predicted dependence of the steady ROS on wind speed,  $u_{10}$ , is depicted quantitatively in fig. 5. Apart from the variation of  $u_{10}$ , all other parameter values are as listed in table 2. It is noted that the numerical results in fig. 5 follow very closely a parabolic curve,  $\text{ROS} = (\text{ROS})_0 + \phi u_{10}^2$ , with  $(\text{ROS})_0$  the rate of spread at zero wind speed. The coefficient  $\phi$  is evidently expected to vary with the fuel properties, as outlined in the previous subsection.

### 3.4. Wildfire development in two-dimensional lattice

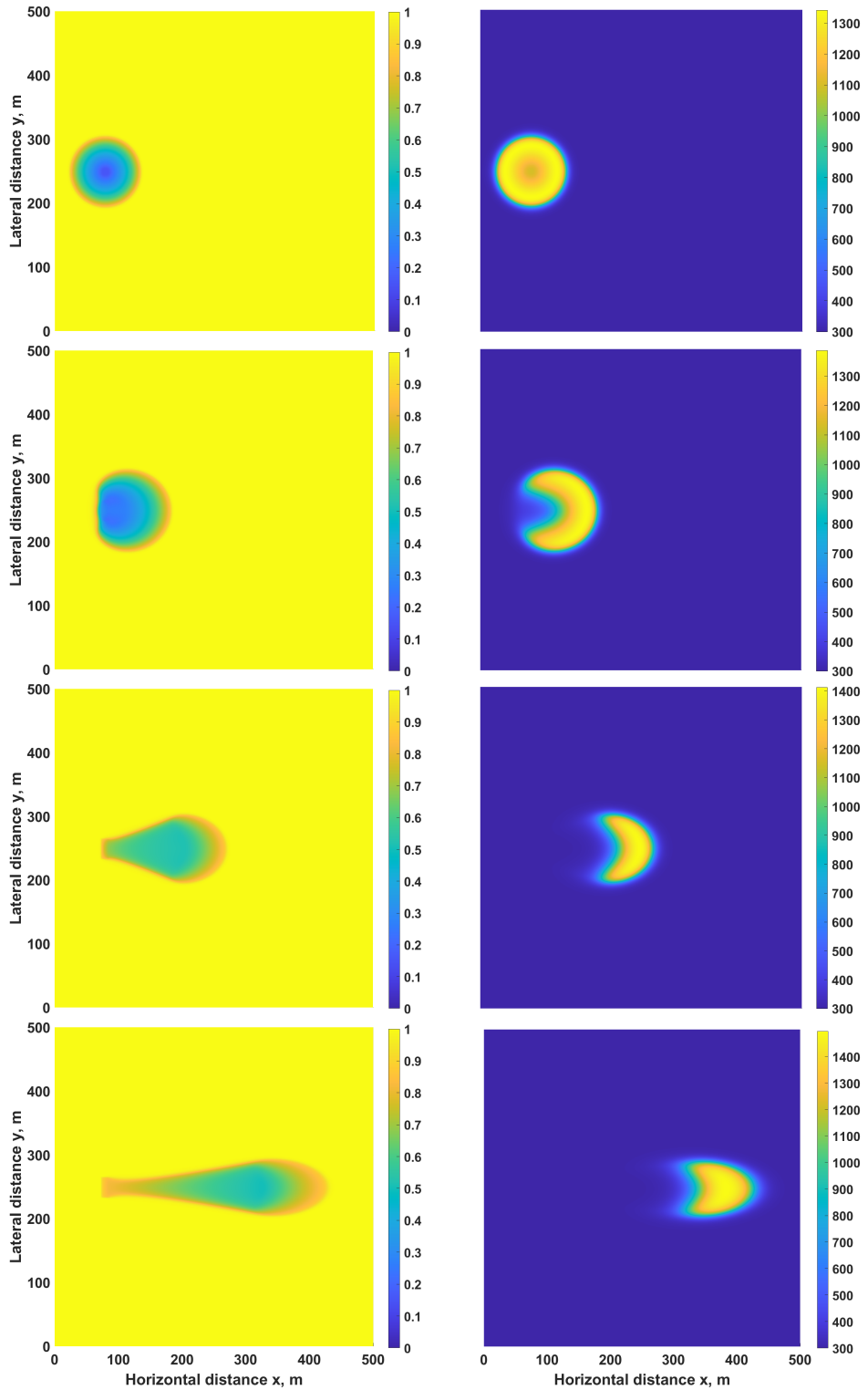
Next, simulations of fire spreading over a two-dimensional field are presented. In all cases considered, the composition and properties of the plantation are assumed to be uniform, and the wind maintains a constant magnitude and direction. The main goal of this section is to compare predictions with field observations on the progression and shape of the fire front in various directions. In most simulations, the fire is ignited by a step-function over a narrow square section (localized ignition). However, high-temperature stripes with varying width in the direction normal to the wind are also considered as an initial condition, in order to investigate the effect of fireline width on its rate of spread.

Figure 6 depicts simulation results for fires developing from a 10 m by 30 m ignition site subject to different wind velocities. The column on the left shows the fraction of solid material (including moisture) that remains on the field after  $t = 900$  s of burning. Thus, it provides an overall view of the area affected by the fire. The column on the right plots the distribution of temperature, and thus it depicts the location and shape of the firefront after a lapse of  $t = 900$  s. The first row in fig. 6 corresponds to  $u_{10} = 0$  m/s, and, as expected, the region affected by the fire is a perfect circle. With increasing wind speed ( $u_{10} = 3, 6$  and  $10$  m/s in the 2nd, 3rd, and 4th rows, respectively), the shape of the fire-affected region becomes gradually more restricted in the transverse direction and far more elongated in the direction of the wind [1]. A striking feature of the left column of fig. 6 is the difference in fuel consumption. Thus, with no-wind, maximum consumption occurs at the ignition site, and relatively little fuel remains there as a consequence of the slow burning process. This trend rapidly diminishes with wind, and at high speeds, the maximum in fuel consumption progresses with the wave front. On the contrary, the ignition site remains rich in fuel.

The change in the firefront location and shape with increasing wind speed is depicted on the right column of fig. 6. As expected, the front moves faster with a stronger wind. Also, the shape varies from symmetric to horseshoe and then to a parabola of increasing steepness. This tendency of the high-temperature zone to progress faster in the direction of the wind than in the transverse direction, which gives rise to the parabolic shape of the firefront, is strongly supported by laboratory and field studies [26, 2, 12]. The evolution of the firefront may be more clearly observed in fig. 7, which depicts the temperature profile for a wind speed of  $u_{10} = 6$  m/s at three time instants,  $t = 0, 900,$  and  $1800$  s from ignition. It shows that the front and the flanks progress with distinctly different speeds, which –in combination with the rapid cooling behind the front by the incoming cold wind– results in the pointed parabolic shape of the fireline. Of course, the semi-burned material left behind is totally dry and will easily ignite if heated again.

The last set of simulations concerns a study of the effect of initial fireline length on the ROS. It is recalled that field studies and simulations converge on the prediction that the ROS is slower for a short fireline and increases asymptotically to a steady-state value with increasing fireline length [10, 6, 22]. It is also recalled that an effect of fireline length has been included in the dispersion coefficient, eq. (8), in an attempt to model this behavior.





**Figure 6:** The state of the burning field 900 s after ignition from a localized source,  $x \in [75, 85]$  m and  $y \in [235, 265]$  m. Left column: the remaining total mass fraction of solid. Right column: The spatial variation of temperature. The rows are (from top to bottom) for  $u_{10} = 0, 3, 6$  and  $10$  m/s.

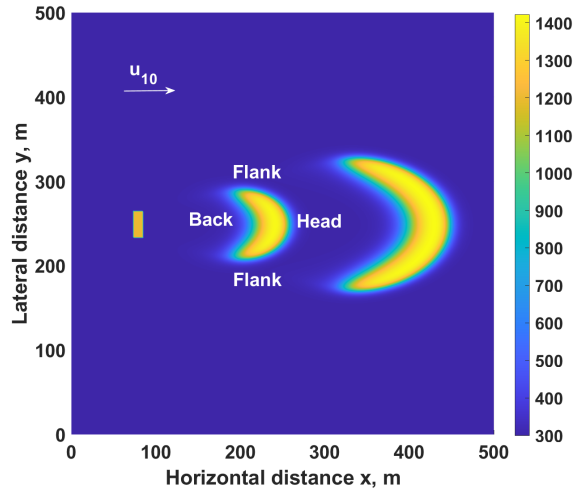


**Figure 7:** Evolution of the temperature profile from the same localized source at three time instants,  $t = 0, 900$  and  $1800$  s, for  $u_{10} = 6$  m/s.

**Table 3**

Best-fit values for the parameters in eq. (30)

Wind speeds $u_{10}$ (m/s)	$a_1$ (m/s)	$a_2$ ( $m^{-1}$ )
3	0.09	$6.91 \cdot 10^{-2}$
6	0.18	$7.93 \cdot 10^{-2}$
10	0.33	$6.72 \cdot 10^{-2}$

Results of the present model are presented in fig. 8. Three different wind speeds,  $u_{10} = 3, 6,$  and  $10$  m/s, are considered, and the initial length of the fireline in the transverse direction (normal to the wind) is varied in the interval  $w \in [5, 200]$  m. It is evident from fig. 8 that, for all cases, the ROS is accurately described by an equation of the form:

$$\text{ROS} = a_1(1 - e^{-a_2 w}), \quad (30)$$

with the best-fit values of the two coefficients given in table 3. Coefficient  $a_1$  ([=] m/s) denotes the asymptotic (quasi-steady-state) velocity of the combustion wave for a long fireline,  $(\text{ROS})_0$ . It is evidently determined by the strength of the wind, which remains the dominant influence [42]. Coefficient  $a_2$  ([=]  $m^{-1}$ ) affects the length,  $w_0$ , of the fireline beyond which the asymptotic value  $(\text{ROS})_0$  is practically reached. According to table 3,  $a_2$  depends very weakly on  $u_{10}$ , and a constant value  $a_2 \approx 7.3 \cdot 10^{-2} m^{-1}$  gives accurate results. By selecting a smaller value for parameter  $\gamma_d$  in eq. (8),  $a_2$  also decreases and the length  $w_0$  increases.

## 4. Conclusions and Outlook

A physically-based, and interpretable model of fire propagation has been developed by combining simplified reaction kinetics with mass and energy balances. The latter includes a convective contribution by the mean gas velocity

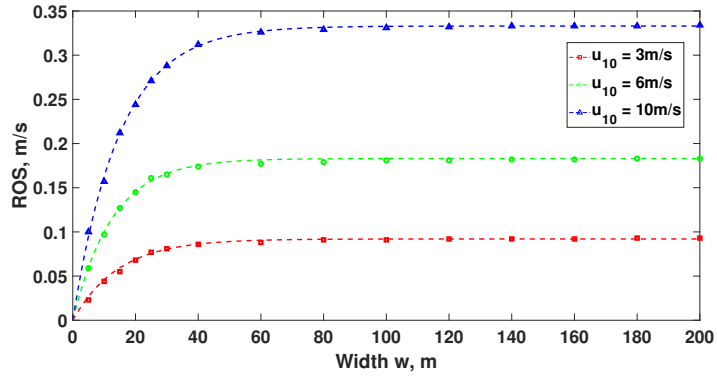


**Figure 8:** The ROS as function of the width,  $w$ , of the fireline for wind speeds  $u_{10} = 3, 6$  and  $10$  m/s. Points are simulation results and lines the best-fit to eq. (30).

through the canopy, a dispersion term that accounts for short-scale heat transfer by turbulence, buoyant currents, and radiation, and a term representing losses to the ambient by free convection and radiation. The mean velocity through the canopy is a key quantity both for the convection and dispersion terms. It is estimated from the effect of ambient wind, quantified by  $u_{10}$ , on the two extremes, (i) air flow through an intact canopy (wind-induced momentum dissipated as canopy drag) and (ii) air flow above totally burned ground (wind-induced momentum dissipated as rough wall drag).

In the present work, an off-line validation of the developed model is attempted by providing predictions for which benchmark data are available in the literature. Concerning fuel properties, it is shown that higher bulk density leads to slower ROS according to the inverse power expression  $ROS \sim m_{s,0}^{-\zeta}$ , as does fuel moisture according to the exponential expression  $ROS \sim e^{-\mu(\text{FMC})}$ . Also, the effect of fuel size (leaves, branches, and trunks) may be quantified by an appropriate choice of the constants in the combustion kinetics.

The effect of ambient wind is considered first for one-dimensional propagation, i.e., for a straight firefront normal to the wind that extends across the entire field. With increasing wind speed, backward propagation of the firefront is decelerated and then extinguished, while propagation along the wind is intensified, varying with the square of the speed,  $u_{10}$ . Fire propagation in a two-dimensional field is considered next, ignited by a localized high-temperature spike, and the spatio-temporal evolution of the firefront and of the fire-affected region is investigated. In particular, the model correctly predicts the effect of wind on increasingly elongating the fire-affected region in the direction of wind and restricting it in the transverse direction. Also, the firefront is predicted to evolve from symmetric to horseshoe to parabolic as a result of the reduced rate of spread of the flanks. Last, the effect of the length of an initial ignition front is investigated, and it is shown that (as a result of the functional form chosen for the dispersion coefficient), the model correctly predicts reduced ROS for short firefronts and an asymptotic approach to the one-dimensional ROS for a long enough firefront.

The aforementioned model is envisioned as a component of a more general data-informed and quick-feedback simulation framework that will assist decisions in the management of wildfires. In particular, the uncertain and stochastic nature of physical features that influence wildfire spread (e.g., fuel properties and weather conditions) will be quantified by an optimal inference process of the model parameters. In future work, it will be attempted to extend the model's applicability by including the effect of terrain topography on the local rate of spread.

## References

- [1] Alexander, M.E., 1985. Estimating the length-to-breadth ratio of elliptical forest fire patterns, in: Proc. of the 8th Conference on Fire and Forest Meteorology, Society of American Foresters, Detroit, MI. Bethesda, MD. pp. 287–304.
- [2] Anderson, H.E., 1983. Predicting wind-driven wild land fire size and shape. Ogden, UT: U.S. Department of Agriculture, Forest Service, Intermountain Forest and Range Experiment Station Res. Pap. INT-305, p. 26.
- [3] Banerjee, T., Heilman, W., Goodrick, S., Hiers, J.K., Linn, R., 2020. Effects of canopy midstory management and fuel moisture on wildfire behavior. *Scientific Reports* 10, 1–14.
- [4] Buerger, R., Inzunza, E.G.D., Mulet, P., Villada, L.M., 2020. Exploring a convection–diffusion–reaction model of the propagation of forest fires: computation of risk maps for heterogeneous environments. *Mathematics* 8, 1674.
- [5] Bürger, R., Gavilán, E., Inzunza, D., Mulet, P., Villada, L.M., 2020. Implicit-explicit methods for a convection-diffusion-reaction model of the propagation of forest fires. *Mathematics* 8, 1034.
- [6] Canfield, J.M., Linn, R.R., Sauer, J.A., Finney, M., Forthofer, J., 2014. A numerical investigation of the interplay between fireline length, geometry, and rate of spread. *Agricultural and Forest Meteorology* 189-190, 48–59.
- [7] Carrier, G., Fendell, F., Wolff, M., 1991. Wind-aided firespread across arrays of discrete fuel elements. I: Theory. *Combustion Science and Technology* 75, 31–51.
- [8] Carvalho, A., Monteiro, A., Flannigan, M., Solman, S., Miranda, A.I., Borrego, C., 2011. Forest fires in a changing climate and their impacts on air quality. *Atmospheric Environment* 45, 5545–5553.
- [9] Catchpole, W.R., Catchpole, E.A., Butler, B.W., Rothermel, R.C., Morris, G.A., Latham, D.J., 1998. Rate of spread of free-burning fires in woody fuels in a wind tunnel. *Combustion Science and Technology* 131, 1–37.
- [10] Cheney, N.P., Gould, J.S., 1995. Fire growth in grassland fuels. *International Journal of Wildland Fire* 5, 237–247.
- [11] Cheney, N.P., Gould, J.S., Catchpole, W.R., 1993. The influence of fuel, weather and fire-shape variables on fire-spread in grasslands. *International Journal of Wildland Fire* 3, 31–44.
- [12] Clark, T.L., Coen, J.L., Latham, D., 2004. Description of a coupled atmosphere–fire model. *International Journal of Wildland Fire* 13, 49–63.
- [13] Coen, J., Cameron, M., Michalakes, J., Patton, E., Riggan, P., Yedinak, K., 2013. Coupled weather–wildland fire modeling with the weather research and forecasting model. *Journal of Applied Meteorology and Climatology* 52, 16–38.
- [14] Coen, J.L., Beezley, J.D., Bennethum, L.S., Douglas, C.C., Kim, M., Kremens, R., Mandel, J., Qin, G., Vodacek, A., 2007. A wildland fire dynamic data-driven application system. 11th Symposium on Integrated Observing and Assimilation Systems for the Atmosphere, Oceans, and Land Surface (IOAS-AOLS) , 3.12.
- [15] Cruz, M., Alexander, M., Fernandes, P., Kilinc, M., Sil, A., 2020. Evaluating the 10% wind speed rule of thumb for estimating a wildfire's forward rate of spread against an extensive independent set of observations. *Environmental Modelling and Software* 133, 104818.
- [16] Cussler, E.L., 2009. *Diffusion: Mass Transfer in Fluid Systems*. 3rd ed., Cambridge University Press, Cambridge, U.K.

- [17] Dhanarathinam, R.S., Kolar, A.K., 2011. Experimental investigation of the effect of initial fuel particle shape, size and bed temperature on devolatilization of single wood particle in a hot fluidized bed. *Journal of Analytical and Applied Pyrolysis* 92, 239–249.
- [18] Dong, S., Karniadakis, G., Chrysosostomidis, C., 2014. A robust and accurate outflow boundary condition for incompressible flow simulations on severely-truncated unbounded domains. *Journal of Computational Physics* 261, 587–608.
- [19] Elhami-Khorasani, N., Ebrahimian, H., Buja, L., Cutter, S.L., Kosovic, B., Lareau, N., Meacham, B.J., Rowell, E., Taciroglu, E., Thompson, M.P., Watts, A.C., 2022. Conceptualizing a probabilistic risk and loss assessment framework for wildfires. *Natural Hazards* 114, 1153–1169.
- [20] Fernandes, P., 2001. Fire spread prediction in shrub fuels in Portugal. *Forest Ecology and Management* 144, 67–74.
- [21] Fernandes, P.M., Botelho, H.S., Rego, F.C., Loureiro, C., 2009. Empirical modelling of surface fire behaviour in maritime pine stands. *Journal of Wildland Fire* 18, 698–710.
- [22] Finney, M.A., 2019. Fire acceleration, in: Manzello, S.L. (Ed.), *Encyclopedia of Wildfires and Wildland-Urban Interface (WUI) Fires*. Springer, Cham, Switzerland, pp. 1–4.
- [23] Finney, M.A., Cohen, J.D., Forthofer, J.M., McAllister, S.S., Gollner, M.J., Gorham, D.J., Saito, K., Akafuah, N.K., Adams, B.A., English, J.D., 2015. Role of buoyant flame dynamics in wildfire spread. *Proceedings of the National Academy of Sciences (PNAS)* 112, 9833–9838.
- [24] Finney, M.A., Cohen, J.D., McAllister, S.S., Jolly, W.M., 2013. On the need for a theory of wildland fire spread. *International Journal of Wildland Fire* 22, 25–36.
- [25] Flannigan, M.D., Stocks, B.J., Wotton, B.M., 2000. Climate change and forest fires. *The Science of the Total Environment* 262, 221–229.
- [26] Fons, W.L., 1946. Analysis of fire spread in light forest fuels. *Journal of Agricultural Research* 72, 92–121.
- [27] Frankman, D., Webb, B.W., Butler, B.W., Jimenez, D., Harrington, M., 2013. The effect of sampling rate on interpretation of the temporal characteristics of radiative and convective heating in wildland flames. *International Journal of Wildland Fire* 22, 168–173.
- [28] Gonçalves, R., Linhares, C., Yojo, T., 2023. Drag coefficient in urban trees. *Trees* 37, 133–145.
- [29] Hairer, E., Nørsett, S., Wanner, G., 1993. *Solving Ordinary Differential Equations I*. 2nd ed., Springer, Heidelberg, Germany.
- [30] Harman, I.N., Finnigan, J.J., 2007. A simple unified theory for flow in the canopy and roughness sublayer. *Boundary-Layer Meteorology* 123, 339–363.
- [31] Harman, I.N., Finnigan, J.J., 2010. Flow over hills covered by a plant canopy: extension to generalised two-dimensional topography. *Boundary-Layer Meteorology* 135, 51–65.
- [32] Huang, X., Gao, J., 2021. A review of near-limit opposed fire spread. *Fire Safety Journal* 120, 103141.
- [33] Inoue, E., 1963. On the turbulent structure of air flow within crop canopies. *Journal of the Meteorological Society of Japan* 41, 317–326.
- [34] Juliano, T.W., Lareau, N., Frediani, M.E., Shamsaei, K., Eghdami, M., Kosiba, K., Wurman, J., DeCastro, A., Kosović, B., Ebrahimian, H., 2021. Toward a better understanding of wildfire behavior in the wildland-urban interface: A case study of the 2021 Marshall fire. *Geophysical Research Letters* 50, e2022GL101557.
- [35] Lareau, N.P., Donohoe, A., Roberts, M., Ebrahimian, H., 2022. Tracking wildfires with weather radars. *Geophysical Research* 127, e2021JD036158.
- [36] Leckner, B., Hansson, K.M., Tullin, C., Borodulya, A.V., Dikalenko, V.I., Palchonok, G.I., 1999. Kinetics of fluidized bed combustion of wood pellets, in: Reuther, R.B. (Ed.), *Proc. 15th International Conference on Fluidized Bed Combustion*, Savannah, GA, US. pp. 15, Paper FBC99.0047.
- [37] Linn, R.R., Cunningham, P., 2005. Numerical simulations of grass fires using a coupled atmosphere–fire model: Basic fire behavior and dependence on wind speed. *Journal of Geophysical Research* 110, D13107.

- [38] Mandel, J., Beezley, J., Kochanski, A., 2011. Coupled atmosphere–wildland fire modeling with wrf 3.3 and sfire. *Geoscientific Model Development* 4, 591–610.
- [39] Mandel, J., Bennethum, L.S., Beezley, J.D., Coen, J.L., Douglas, C.C., Kim, M., Vodacek, A., 2008. A wildland fire model with data assimilation. *Mathematics and Computers in Simulation* 79, 584–606.
- [40] Marino, E., Dupuy, J.L., Pimont, F., Guijarro, M., Hernando, C., Linn, R.R., 2012. Fuel bulk density and fuel moisture content effects on fire rate of spread: a comparison between firetec model predictions and experimental results in shrub fuels. *Journal Fire Sciences* 30, 277–299.
- [41] McCarthy, N., Guyot, A., Dowdy, A., McGowan, H., 2019. Wildfire and weather radar: A review. *Geophysical Research* 41, 266–286.
- [42] Mell, W., Jenkins, M.A., Gould, J., Cheney, P., 2007. A physics-based approach to modelling grassland fires. *International Journal Wildland Fire* 16, 1–22.
- [43] Moinuddin, K., Khan, N., Sutherland, D., 2021. Numerical study on effect of relative humidity (and fuel moisture) on modes of grassfire propagation,. *Fire Safety Journal*, 125.
- [44] Morvan, D., Dupuy, J., 2004. Modeling the propagation of a wildfire through a mediterranean shrub using a multiphase formulation. *Combustion and Flame* 138, 199–210.
- [45] Nelson, R.M., Adkins, C.W., 1988. A dimensionless correlation for the spread of wind-driven fires. *Canadian Journal of Forest Research* 18, 391–397.
- [46] Papanastasiou, T., Malamataris, N., Ellwood, K., 1992. A new outflow boundary condition. *International Journal for Numerical Methods in Fluids* 14, 587–608.
- [47] Pastor, E., Zárate, L., Planas, E., Arnaldos, J., 2003. Mathematical models and calculation systems for the study of wildland fire behaviour. *Progress in Energy and Combustion Science* 29, 139–153.
- [48] Paugam, R., Wooster, M.J., Roberts, G., 2012. Use of handheld thermal imager data for airborne mapping of fire radiative power and energy and flame front rate of spread. *IEEE TRANSACTIONS ON GEOSCIENCE AND REMOTE SENSING* 51, 3385–3399.
- [49] Pimont, F., Dupuy, J.L., Caraglio, Y., Morvan, D., 2009. Effect of vegetation heterogeneity on radiative transfer in forest fires. *International Journal of Wildland Fire* 18, 536–553.
- [50] Pimont, F., Dupuy, J.L., Linn, R.R., 2012. Coupled slope and wind effects on fire spread with influences of fire size: a numerical study using firetec. *International Journal of Wildland Fire* 21, 828–842.
- [51] Rossa, C.G., 2017. The effect of fuel moisture content on the spread rate of forest fires in the absence of wind or slope. *International Journal of Wildland Fire* 26, 24–31.
- [52] Santoso, M.A., Christensen, E.G., Yang, J., Rein, G., 2019. Review of the transition from smouldering to flaming combustion in wildfires. *Frontiers in Mechanical Engineering* 5.
- [53] Seron, F.J., Gutierrez, D., Magallon, J., Ferragut, L., Asensio, M.I., 2005. The evolution of a WILDLAND forest FIRE FRONT. *The Visual Computer* 41, 152–169.
- [54] Silva, J., Marques, J., Gonçalves, I., Brito, R., Teixeira, S., Teixeira, J., Alvelos, F., 2022. A systematic review and bibliometric analysis of wildland fire behavior modeling. *Fluids* 7, 139–153.
- [55] Simeoni, A., Santoni, P.A., Larini, M., Balbi, J.H., 2001. On the wind advection influence on the fire spread across a fuel bed: modelling by a semi-physical approach and testing with experiments. *Fire Safety Journal* 36, 491–513.
- [56] Simeoni, A., Santoni, P.A., Larini, M., Balbi, J.H., 2011. Physical modelling of forest fire spreading through heterogeneous fuel beds. *International Journal of Wildland Fire* 20, 625–632.
- [57] Speer, K., Goodrick, S., 2022. *Wildland Fire Dynamics*. 1st ed., Cambridge University Press, Cambridge, U.K.

- [58] Stull, R., 2017. *Practical Meteorology: An Algebra-based Survey of Atmospheric Science*. University of British Columbia, Vancouver, BC, Canada. Available online: [https://www.eoas.ubc.ca/books/Practical\\_Meteorology](https://www.eoas.ubc.ca/books/Practical_Meteorology).
- [59] Sullivan, A., 2017. Inside the inferno: Fundamental processes of wildland fire behaviour. part 1: Combustion chemistry and energy release. *Current Forestry Reports* 3, 132–149.
- [60] Sullivan, A.L., 2009. Wildland surface fire spread modelling, 1990–2007. 1: Physical and quasi-physical models. *International Journal of Wildland Fire* 18, 349–368.
- [61] Taylor, S.W., Wotton, B.M., Alexander, M.E., Dalrymple, G.N., 2004. Variation in wind and crown fire behaviour in a northern jack pine black spruce forest. *Canadian Journal of Forest Research* 34, 1561–1576.
- [62] Thomas, P.H., 1971. Rates of spread of some wind-driven fires. *Forestry* 44, 155–175.
- [63] Vega, J.A., Cuinas, P., Fonturbel, J., Perez-Gorostiara, P., Fernandez, C., 1998. Predicting fire behaviour in galician (nw spain) shrubland fuel complexes. *Proc. 3rd International Conference of Forest Fire Research and 14th Conference of Fire Forest Meteorology* 2, 16–20.
- [64] Weise, D.R., Biging, G.S., 1997. A qualitative comparison of fire spread models incorporating wind and slope effects. *Forest Science* 43, 170–180.
- [65] Wolff, M.F., Carrier, G.F., Fendell, F.E., 1991. Wind-aided firespread across arrays of discrete fuel elements. II. Experiment. *Combustion Science and Technology* 77, 261–289.